# Bouc-Wen modelling of asymmetric Stockbridge damper for suspension bridge hangers

Giacomo Bacci[1], Ø. W. Petersen[1], V. Denoël[2], O. A. Øiseth[1]

[1] *NTNU, Norwegian University of Science and Technology, 7491 Trondheim, Norway*
[2] *ULiège, University of Liège, 4000 Liège, Belgium*

giacomo.bacci@ntnu.no, oyvind.w.petersen@ntnu.no, v.denoel@uliege.be, ole.oiseth@ntnu.no

***Abstract***— Stockbridge dampers are increasingly adopted for mitigating wind-induced vibrations of suspension bridge hangers, where their size and vertical installation differ substantially from traditional overhead-line applications. Recent works reported cases of premature failure of these devices for this kind of application [1], [2]. Existing modelling approaches are often calibrated for smaller, symmetric devices and rely on linear or black-box representations. This paper presents a nonlinear dynamic model for asymmetric Stockbridge dampers intended for bridge applications, aimed at preserving physical interpretability while remaining suitable for system-level simulations. The formulation employs a four degree-of-freedom representation in which the hysteretic bending behaviour of the messenger cables is captured through Bouc–Wen–type constitutive laws expressed in suitably defined generalised coordinates. Model parameters are identified from laboratory tests on a full-scale damper installed in a vertical configuration representative of field conditions. The calibrated model reproduces the amplitude-dependent shift of resonance frequencies and the variation of force transmission observed experimentally, without resorting to amplitude-specific impedance functions. Validation against both harmonic and broadband excitations demonstrates the capability of the model to predict the transmitted force and internal damper dynamics over a wide frequency range. Compared to conventional impedance-based approaches, the proposed framework enables consistent treatment of nonlinear effects under arbitrary excitation histories and provides a practical tool for integration into hanger–damper vibration analyses.

Keywords— ***Stockbridge damper, Bouc-Wen, Nonlinear model, Experimental calibration***

## 1 Damper modelling framework

Stockbridge dampers have been studied extensively in the context of overhead transmission lines, where their nonlinear dynamic behaviour has long been recognised as a key factor governing vibration mitigation performance. Early analytical models of Stockbridge dampers idealised the device as a linear two-degree-of-freedom system subjected to base excitation, where the messenger cable behaviour is represented through equivalent linear stiffness and hysteretic damping [3]. While this approach captures the main resonant behaviour, it does not account for the amplitude-dependent dynamics observed in practice. Early phenomenological approaches, such as those introduced by Pivovarov and Vinogradov [4], employed Bouc–Wen–type hysteresis models to represent the amplitude-dependent stiffness and energy dissipation of the messenger cable in a single-degree-of-freedom formulation. Subsequent developments by Sauter and co-workers [5] introduced beam-based descriptions of the messenger cable with hysteretic moment–curvature relationships, enabling a closer connection between experimental observations and structural mechanics. Building on the extensive experimental work of Sauter [6], Foti et al. [7] proposed a sectional Bouc-Wen model suitable for dynamic simulations. Finite-element modelling has also been used with different kinds of elements and levels of approximation [8]–[11], to culminate with the high-fidelity representation of Luo [12], incorporating contact and friction effects at the wire level with nonlinear 3D elements. More recently, Bogani [13] proposed a preliminary version of a two degrees-of-freedom global Bouc-Wen model for a Stockbridge damper in overhead line applications.

Despite these advances, all the mentioned formulations have been developed for dampers tested in horizontal configurations and calibrated for overhead-line applications. The modelling of large, asymmetric Stockbridge dampers installed vertically on suspension bridge hangers, therefore, remains comparatively underexplored. The formulation

presented here addresses this gap by introducing a four degrees-of-freedom nonlinear Bouc-Wen model tailored to asymmetric devices and suitable for direct integration into hanger–damper simulations.

### 1.1 Governing equations

We consider an asymmetric Stockbridge damper composed of a rigid clamp and two rigid inertial masses connected to the clamp by flexible messenger cables of different lengths. The damper is installed vertically, as in typical suspension bridge applications, with the clamp rigidly attached to the hanger. Motion is restricted to a vertical plane perpendicular to the wind direction, consistent with the dominant direction of vortex-induced vibrations in hangers. Fig. 1a shows a scheme of the considered damper. The excitation of the damper is provided by the horizontal displacement of the clamp, denoted by $y_c(t)$. Each inertial mass $i \in \{1,2\}$ is described by two in-plane degrees of freedom: the horizontal displacement of its centre of gravity relative to the clamp, $d_{COG_i}(t)$, and the rotation of the mass about its centroid, $\theta_i(t)$. The absolute horizontal displacement of the centre of mass is therefore written as

$$x_{COG_i}(t) = y_c(t) + d_{COG_i}(t) \tag{1}$$

The messenger cables transmit to each mass a horizontal shear force $F_i(t)$ and a bending moment $M_i(t)$ at the cable–mass interface (Fig. 1b). These internal actions arise from the bending deformation of the messenger cable and are responsible for both stiffness and energy dissipation. The mass of the messenger cable is neglected, as it is small compared to the attached inertial masses. The equations of motion are obtained by enforcing the dynamic equilibrium of each rigid mass. This leads to the following equations of motion.

$$m_i \ddot{d}_{G_i}(t) + F_i(t) = -m_i\, \ddot{y}_c(t) \tag{2}$$

$$J_i\, \ddot{\theta}_i(t) + M_i(t) - \eta_i\, e_{COG_i}\, F_i(t) = 0 \tag{3}$$

Where $m_i$ is the mass of the $i$-th inertial body and the right-hand side represents the inertial forcing induced by the imposed clamp acceleration. $J_i$ is the mass moment of inertia of the body, $e_{COG_i}$ is the distance between the cable attachment point and the centroid, and $\eta_i = (-1)^{i+1}$ is a sign factor accounting for the opposite orientation of the two masses with respect to the clamp. Eq. 4 defines the force that the damper exchanges through the clamp to the hanger cable.

$$F_c = m_c \ddot{y}_c - (F_1 + F_2) \tag{4}$$

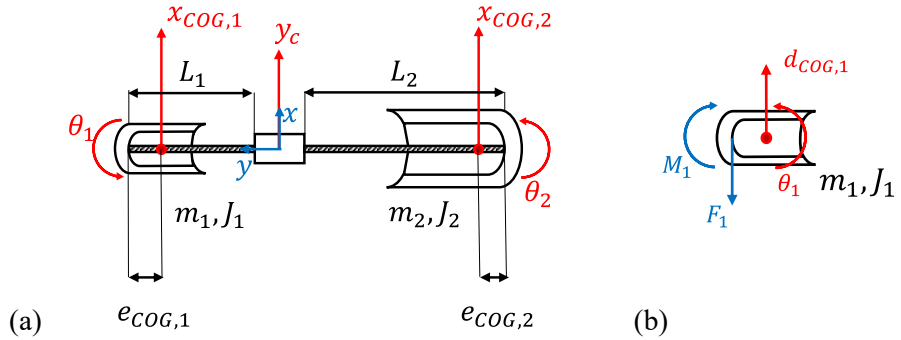


**Fig. 1** a) Modelling scheme of a four degrees-of-freedom Stockbridge damper. b) Force equilibrium of the top mass.

Eq. 2 and 3 describe the coupled translational and rotational dynamics of each inertial mass driven by the clamp motion and resisted by the nonlinear reaction forces of the messenger cables. The force $F_i$ and moment $M_i$ represent the complex hysteretic behaviour of the stranded cable.

The original formulation of the Bouc–Wen model was originally conceived for systems with a single internal variable [14]; several extensions to higher-dimensional settings have been proposed in the literature. These multi-dimensional formulations, however, often require additional nonlinear coupling terms that complicate both parameter identification and physical interpretation. In the present work, such complexity is deliberately avoided. The dynamic behaviour of a Stockbridge damper is characterised by a small number of well-separated resonance phenomena, each associated with large-amplitude motion of the inertial masses involving different combinations of translation and rotation. Experimental

observations indicate that interactions between these resonant mechanisms are weak, making a fully coupled nonlinear formulation unnecessary for the intended level of description.
Motivated by this observation and drawing an analogy with modal decomposition in linear structural dynamics, the response of each inertial mass is described using two independent generalised coordinates, denoted $q_{1,i}(t)$and $q_{2,i}(t)$. These coordinates are defined as linear combinations of the relative horizontal displacement of the mass centroid $d_{COG_i}(t)$ and its rotation $\theta_i(t)$, as shown in Eq. 5.

$$\begin{pmatrix} d_{COG_i} \\ \theta_i \end{pmatrix} = \begin{bmatrix} 1 & a_i \\ b_i & 1 \end{bmatrix} \begin{pmatrix} q_{1,i} \\ q_{2,i} \end{pmatrix} = \boldsymbol{\phi}_i \begin{pmatrix} q_{1,i} \\ q_{2,i} \end{pmatrix} \tag{5}$$

Here, $\boldsymbol{\phi}_i$is a transformation matrix parameterised by two coefficients $a_i$ and $b_i$, which quantify the relative contribution of translation and rotation in the deformation patterns associated with the dominant resonances of each mass. The $a_i$ and $b_i$ parameters are identified from experimental data. Substituting Eq. 5 into Eq. 2 and 3, the equation of motion of each mass $i$ can be rewritten in terms of the generalised coordinates as in Eq. 6.

$$\boldsymbol{\phi}_i^{\mathrm{T}} \begin{bmatrix} m_i & 0 \\ 0 & J_i \end{bmatrix} \boldsymbol{\phi}_i \begin{pmatrix} \ddot{q}_{1,i} \\ \ddot{q}_{2,i} \end{pmatrix} = -\begin{pmatrix} \tilde{F}_{1,i} \\ \tilde{F}_{2,i} \end{pmatrix} + \boldsymbol{\phi}_i^{\mathrm{T}} \begin{pmatrix} -m_i \ddot{y}_c \\ 0 \end{pmatrix} \tag{6}$$

Here $\tilde{F}_{1,i}$and $\tilde{F}_{2,i}$denote the restoring forces associated with the generalised coordinates $q_{1,i}$and $q_{2,i}$, respectively. These forces represent the nonlinear contribution of the messenger cable expressed in the transformed coordinate system. To capture the amplitude-dependent behaviour of the messenger cable, each generalised force $\tilde{F}_{j,i}$ is modelled using a Bouc–Wen framework. For each mass $i$ and generalised coordinate $j \in \{1,2\}$, the restoring force is expressed as

$$\tilde{F}_{j,i} = k_{j,i}^{\min} q_{j,i} + \left(k_{j,i}^{\max} - k_{j,i}^{\min}\right) c_{j,i} z_{j,i} \tag{7}$$

where $q_{j,i}(t)$ is the generalised displacement and $z_{j,i}(t)$ is a dimensionless internal hysteretic variable. The parameters $k_{j,i}^{\max}$ and $k_{j,i}^{\min}$ represent, respectively, the high- and low-amplitude limits of the effective stiffness associated with each generalised coordinate, while $c_{j,i}$ defines the characteristic displacement level at which the transition between these regimes occurs. Eq. 8 shows the first-order differential equation that rules the evolution of the hysteretic variable.

$$\dot{z}_{j,i} = \frac{1}{c_{j,i}} \left[1 - \operatorname{sgn}\left(\dot{q}_{j,i}\right) z_{j,i}\right] \dot{q}_{j,i} \tag{8}$$

This reduced Bouc-Wen formulation has been shown in previous studies to provide sufficient flexibility for modelling Stockbridge damper dynamics while keeping the number of parameters minimal [13].
In the small-amplitude regime, when $| q_{j,i} | \ll c_{j,i}$, the restoring force is approximately linear with stiffness $k_{j,i}^{\max}$and negligible energy dissipation. As the vibration amplitude increases and the displacement approaches $c_{j,i}$, the hysteretic component becomes active, leading to a progressive reduction of the effective stiffness toward $k_{j,i}^{\min}$ and to an increase in energy dissipation. This mechanism reproduces the experimentally observed softening behaviour of the damper and the amplitude-dependent shift of its resonance characteristics.
With two generalised coordinates per mass and an asymmetric configuration, the present formulation requires three parameters for each $(j,i)$ pair, resulting in a total of twelve hysteretic parameters. Because the transformation matrix depends on the coefficients $a_i$and $b_i$, the calibrated model parameters are sensitive to their values. These coefficients are therefore adjusted as part of the experimental identification process. Once the value of the parameters has been fixed, the system in Eq. 6 is then rewritten in state-space formulation and integrated in time to obtain the time history of the generalised state variables given an imposed clamp motion $y_c(t)$.

## 2 Experimental characterisation and parameter tuning

### 2.1 Laboratory testing description

An asymmetric Stockbridge damper specimen has been retrieved from the Hålogaland suspension bridge in Norway. Geometrical and inertial characteristics of the damper are summarised in Table 1. An experimental campaign was conducted to characterise its dynamic behaviour. The objective of the tests was to identify the force–velocity relationship at the clamp over a broad frequency range and for different excitation amplitudes, thereby providing a reference for model calibration and validation.

The damper was mounted vertically in a laboratory setup representative of its in-service configuration on a bridge hanger. A modal vibration shaker was used to impose a prescribed horizontal motion at the clamp, while the damper masses were left free to respond dynamically. The clamp was connected to the shaker through a low-friction guiding system, and the reaction force transmitted by the damper was measured using load cells integrated into the clamp assembly. A picture and a schematic overview of the setup are shown in Fig. 2.

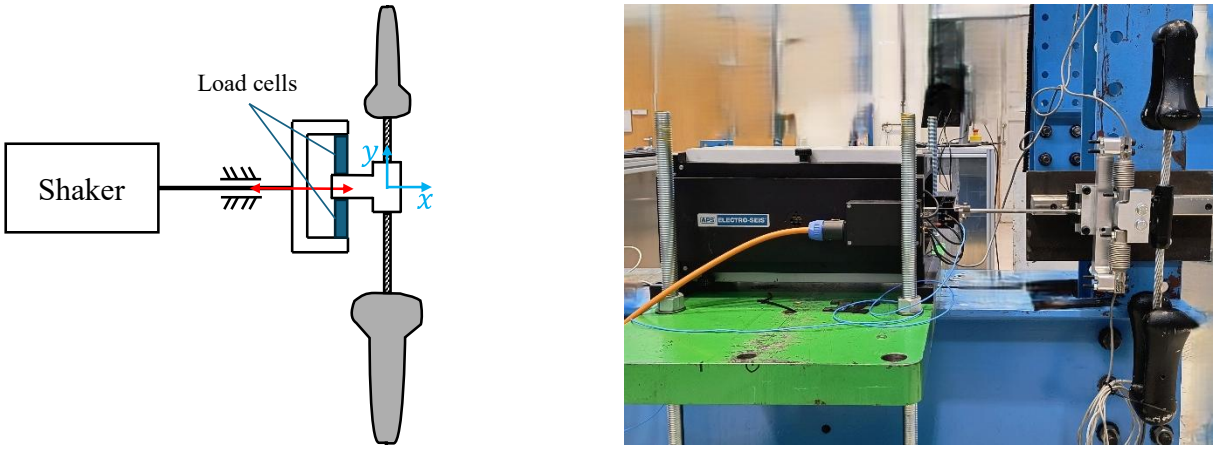


(a) (b)

**Fig. 2** a) Schematic overview of the experimental setup. b) Picture of the experimental setup.

**Table 1** Geometric and inertial parameters of the selected damper.

| Parameter | Symbol | Value |
|---|---|---|
| Top mass | $m_1$ | 4.6 kg |
| Bottom mass | $m_2$ | 7.7 kg |
| Mass of the clamp | $m_c$ | 0.931 kg |
| Rotational inertia of top mass (about centroid) | $J_1$ | 0.02145 kg·m² |
| Rotational inertia of bottom mass (about centroid) | $J_2$ | 0.05234 kg·m² |
| Distance from tip of messenger cable to centroid (top mass) | $e_{COG,1}$ | 0.034 m |
| Distance from tip of messenger cable to centroid (bottom mass) | $e_{COG,2}$ | 0.040 m |

The shaker was operated in acceleration control to generate input signals with approximately constant clamp velocity amplitude, in line with the procedure described in the European Standard for Overhead lines [15]. Logarithmic sine sweeps covering the frequency range of interest were applied at several target velocity levels. The selected velocity amplitudes range from 0.01 m/s to 0.05 m/s, based on vibration levels observed during field measurements on bridge hangers [2]. While the European Standard for overhead lines recommends mono-amplitude tests at a clamp-velocity level of 0.2 m/s, the present study adopts lower amplitudes to reflect the operational conditions of Stockbridge dampers in suspension-bridge applications. This choice accounts for the different installation configuration and excitation levels encountered in bridge hangers compared to overhead power lines.

For each test, the time histories of clamp velocity $y_c(t)$ and transmitted force $F_c(t)$, as well as the internal dynamics of the damper ($d_{COG_i}(t), \theta_i(t)$) were recorded. The damper response is quantified in terms of mechanical impedance at the clamp in the frequency domain. This is consistent with the energy-based framework commonly adopted in standardised testing procedures, in which damper performance is evaluated through the balance between input energy and dissipated energy in the cable–damper system [16], [17], [18]. For a harmonic excitation at angular frequency $\omega$, the impedance is defined as

$$Z(j\omega) = \frac{F_{c0}(j\omega)}{V_c(j\omega)} \tag{9}$$

where $F_c$ and $V_c$ denote the complex amplitudes of the clamp force and clamp velocity, respectively. Applying this procedure to the sine sweep data yields frequency-dependent impedance functions for each excitation amplitude. These

functions are shown in Fig. 3 and they constitute the primary experimental output of the testing campaign. They exhibit four distinct resonance peaks whose frequencies and magnitudes vary systematically with the imposed clamp velocity amplitude, reflecting the softening behaviour and amplitude dependence inherent to the messenger cable mechanics. Such amplitude-dependent shifts of the resonance frequencies have been reported in previous experimental studies on Stockbridge dampers and are consistent with the nonlinear behaviour observed in the present measurements [16], [19]. In Fig. 3a, the locus of the four peaks of the impedance functions is highlighted with a broken line. This is used in the following sections to tune the model's parameters.

From the trends highlighted in Fig. 3a, it can be observed that for clamp-velocity amplitudes exceeding approximately 0.05 m/s, the resonance peaks exhibit progressively smaller shifts toward lower frequencies, while their magnitudes continue to increase. This indicates that, for the investigated damper, the nonlinear behaviour manifests primarily through frequency shifts at low velocity amplitudes and through amplitude amplification at higher levels. Consequently, the amplitude-dependent softening behaviour of the device is most clearly observable at low excitation levels. If only high-amplitude tests, such as the mono-amplitude excitation at 0.2 m/s recommended by the standard, had been performed, the nonlinear response would have been more difficult to identify, as the resonance peaks would have evolved predominantly in magnitude rather than in frequency.

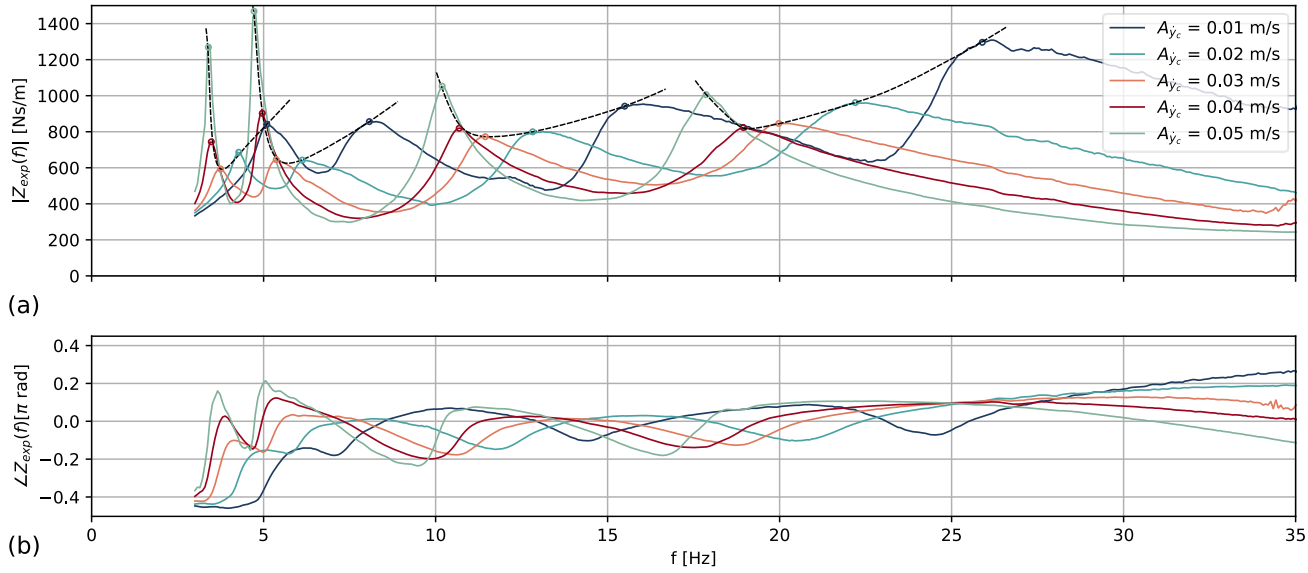


**Fig. 3** Magnitude and phase of the experimentally obtained impedance $\boldsymbol{Z_{exp}(f)}$ for five prescribed clamp velocity levels. Dashed black curves highlight the amplitude-dependent evolution of the resonance peaks.

## 2.2 Identification of model parameters

In Fig. 4, the locus of the peaks of the experimental impedance functions is compared with the numerically derived one. An initial estimate of the stiffness parameters $k_{j,i}^{\max}$ and $k_{j,i}^{\min}$ was obtained by associating the upper and lower frequency limits of each trajectory with the high- and low-amplitude stiffness bounds of the model. The transition parameter governing the onset of nonlinear behaviour $c_{j,i}$ was inferred from the excitation level at which the peak frequency departs from its upper bound and begins to shift toward lower values.

Thanks to the formulation in generalised coordinates, the four dominant resonances of the asymmetric damper could be treated independently during the identification process. This decoupling allows each hysteretic element to be calibrated using a small set of parameters, significantly simplifying the tuning procedure. The transformation coefficients linking physical and generalised coordinates were adjusted concurrently to ensure consistency between the experimentally observed deformation patterns and the numerical response.

The calibration was refined through iterative time-domain simulations of the damper response to the same sine sweep excitations used in the laboratory tests, until satisfactory agreement was achieved between experimental and numerical peak trajectories. The final parameter set is shown in Table 2. The resulting numerical impedance functions, shown in

Fig. 5, closely match the experimentally measured counterparts in Fig. 3 and confirm the ability of the proposed model to capture the dominant nonlinear features of the damper response.

**Table 2** Calibrated parameters of the proposed nonlinear Bouc-Wen Stockbridge damper model derived from experimental impedance data.

| | Top mass translation ($i = 1, j = 1$) | Top mass rotation ($i = 1, j = 2$) | Bottom mass translation ($i = 2, j = 1$) | Bottom mass rotation ($i = 2, j = 2$) |
|---|---|---|---|---|
| $k_{ji}^{min}$ | 4600 | 230 | 4800 | 140 |
| $k_{ji}^{max}$ | 14500 | 500 | 12700 | 480 |
| $c_{ji}$ | 0.00036 | 0.0025 | 0.00055 | 0.0021 |
| $a_i$ | 0.01 | – | –0.001 | – |
| $b_i$ | – | –7 | – | 7 |

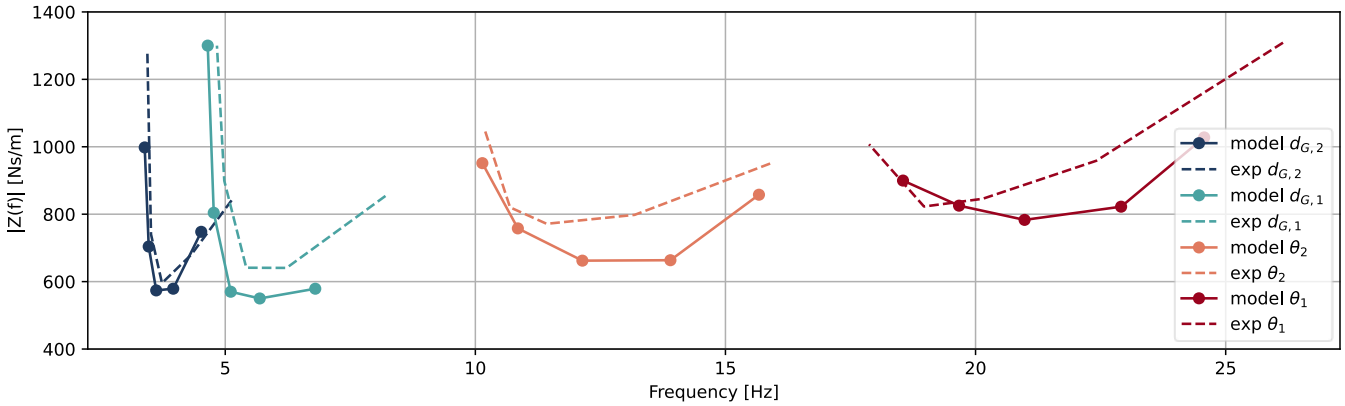


**Fig. 4** Locus of the four dominant resonance peaks of the damper impedance. Experimental results are shown with dashed lines, while solid curves correspond to the response predicted by the calibrated Bouc–Wen model.

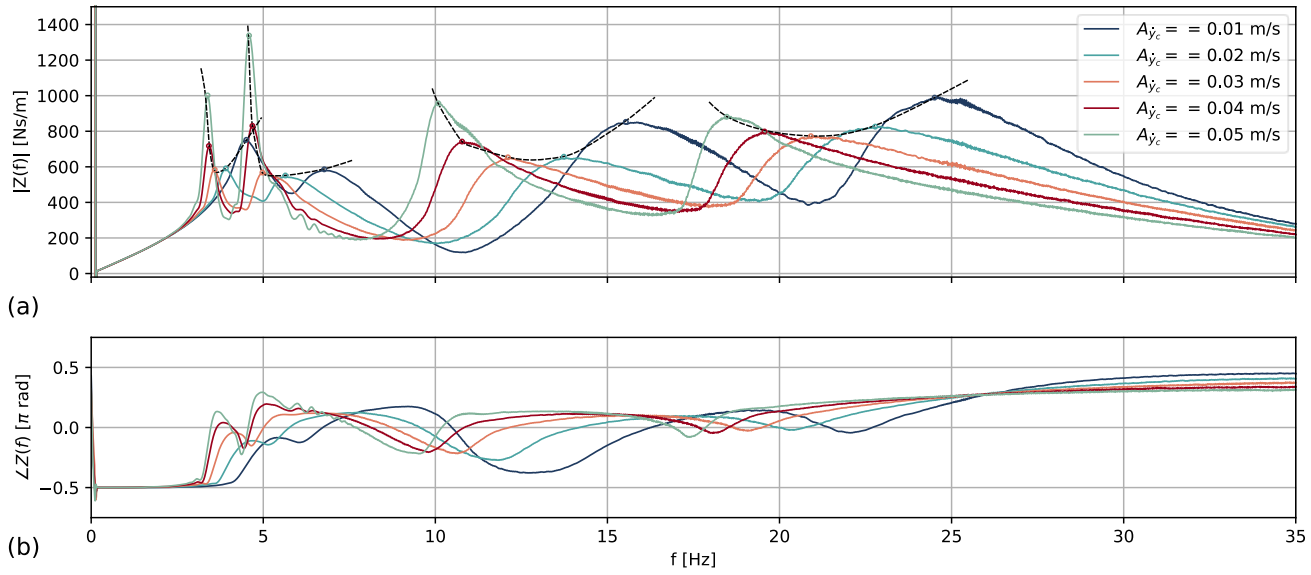


**Fig. 5** Magnitude and phase of the simulated impedance $\boldsymbol{Z}_{\mathbf{num}}(\boldsymbol{f})$ computed for five clamp velocity amplitudes using the model parameters reported in Table 4. Dashed black lines indicate the systematic shift of the resonance peaks with increasing excitation level.

# 3 Relation with existing standards and analytical models

## 3.1 Generic input-output reconstruction

In current engineering practice, Stockbridge dampers are typically characterised through laboratory identification of their mechanical impedance at the clamp, obtained from mono-amplitude harmonic or sine-sweep tests. Once identified, this impedance function is treated as a linear transfer function and used to estimate the transmitted force under operational conditions. While this approach is well established and codified in standards for overhead transmission lines, it works as a black box approach and inherently neglects the amplitude-dependent nonlinear behaviour. To assess the capability of the proposed nonlinear model to go beyond this framework, the damper response was evaluated under multiharmonic excitation representative of field conditions. A clamp-motion time history recorded on a suspension-bridge hanger was reproduced in the laboratory using the same experimental setup employed for parameter identification. The signal contained energy distributed over multiple frequency bands, simultaneously exciting all four resonances of the damper. Despite being calibrated exclusively using monoharmonic sine-sweep tests, the Bouc–Wen model accurately reconstructed both the transmitted clamp force and the internal dynamics of the damper masses when subjected to this multiharmonic input. The simulated time histories and spectra in Fig. 6 showed close agreement with experimental measurements across the frequency range of interest. In particular, the model correctly captured the relative contribution of the translational and rotational degrees of freedom of both masses, demonstrating its ability to represent the coupled internal dynamics governing energy dissipation. This result is significant in view of practical applications. Unlike linear black-box approaches, which provide only an external input–output relation, the proposed formulation allows direct access to internal variables such as mass displacements and rotations. These quantities are essential for assessing stress levels in the messenger cables and for investigating fatigue-related failure mechanisms, which are of particular concern in bridge applications.

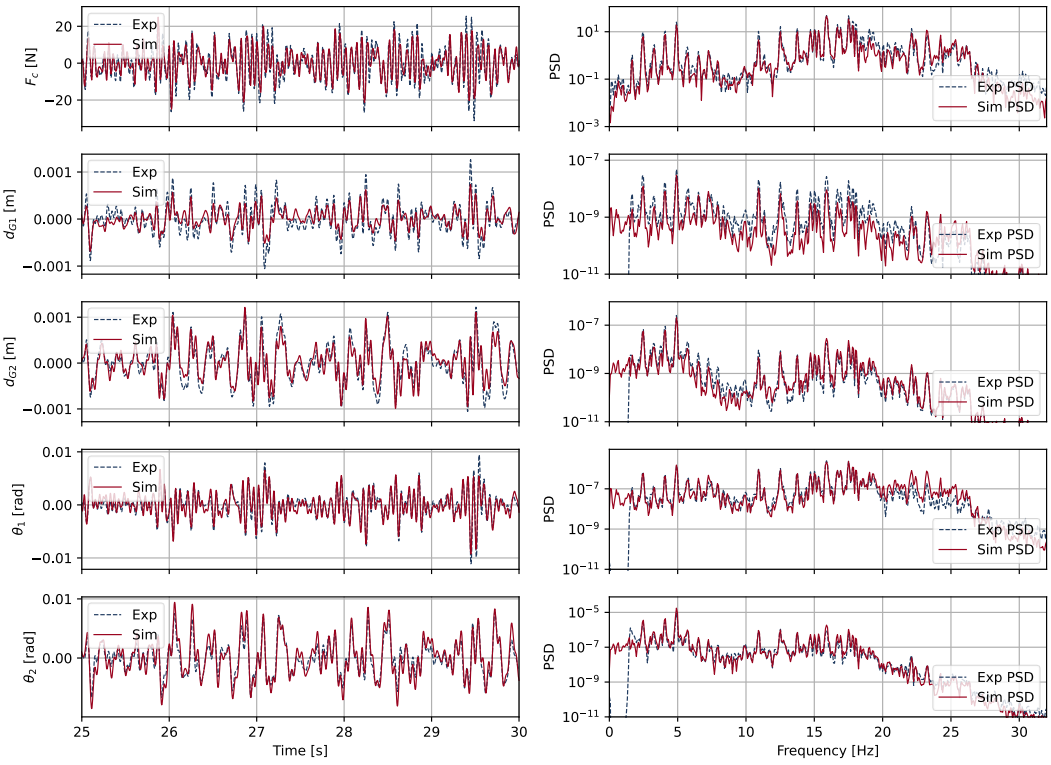


**Fig. 6** Response of the numerical model compared with experimental measurements in both the time and frequency domains for a multiharmonic input.

### 3.2 Other impedance-based models in literature

To further validate the model, the formulation developed in this work can be straightforwardly reduced to the symmetric configuration, in which the two inertial masses are identical, and the messenger cables have equal length. This reduction is achieved by enforcing identical model parameters for the upper and lower masses, except for the scaling parameters, which must assume opposite signs ($a_2 = -a_1$, $b_2 = -b_1$) to account for the opposite orientation of the two masses. This symmetry enables direct comparison with analytical models available in the literature. The reduced formulation was validated against the experimental benchmark data of a symmetric damper for overhead powerline application reported by Sauter et al. [6], which provides measurements of the real part of the mechanical impedance for two different clamp-velocity amplitudes. Model parameters were identified following the same procedure adopted for the asymmetric case and are reported in Table 3. Unlike the previous calibration, an initial estimate for the two scaling parameters was not available for this benchmark. Therefore, the values identified for the asymmetric damper were used as an initial guess and subsequently refined through iterative adjustment. The impedance predicted by the proposed model is compared with two recent analytical formulations by Foti et al. [7] and Bogani et al. [13]. In Foti et al.'s approach, the messenger cable is modelled as an Euler–Bernoulli beam, whose sectional moment–curvature relationship is governed by a Bouc–Wen hysteresis law. Bogani et al., on the other hand, proposed a reduced global Bouc–Wen formulation conceptually closer to the present work. However, in their model the equations of motion are written directly in terms of tip displacement and rotation, and the inertial coupling between these degrees of freedom is neglected. In the context of the present formulation, this assumption corresponds to omitting the inertial coupling term and adopting a diagonal transformation matrix, resulting in a complete decoupling of translational and rotational contributions to the impedance. Consequently, model parameters are identified by fitting individual resonance peaks independently.
In contrast, the formulation proposed here retains all inertial terms and applies the Bouc–Wen hysteresis model in the space of generalised coordinates. This allows the coupled dynamics of all degrees of freedom to be represented consistently within a single framework. The experimental data used for the comparison are the same benchmark measurements employed by both Bogani et al. and Foti et al. in their work.

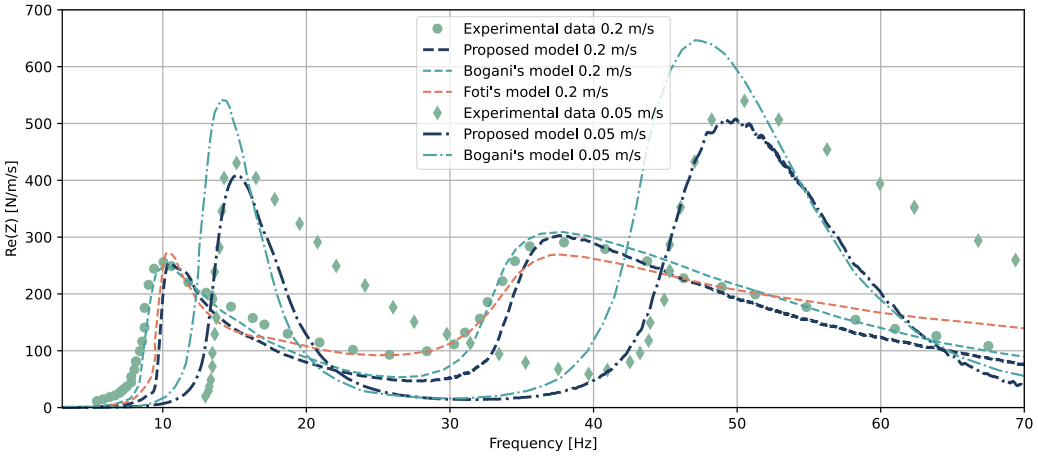


**Fig. 7** Real part of the impedance for a symmetric Stockbridge damper at two clamp-velocity amplitudes: comparison between the proposed model, literature models, and experimental data.

As shown in Fig. 7, the proposed model accurately reproduces the experimental impedance for a clamp-velocity amplitude of 0.2 m/s, which was used for parameter tuning. Both the present formulation and the model by Bogani et al. capture the amplitude-dependent variation of the impedance, whereas this feature is not explicitly reproduced by the original formulation of Foti et al. It should be emphasised that the results for the latter two models are taken directly from the literature and compared against the same experimental data, without any re-identification of parameters.
While the proposed model is formulated to accommodate asymmetric dampers, its reduction to the symmetric case retains the same number of parameters as the model by Bogani et al., namely six in total, with three associated with each degree of freedom. By contrast, the formulation by Foti et al. requires identification of multiple sectional parameters along the messenger cable, leading to a substantially larger parameter set. Despite its compact

parametrisation, the present model demonstrates improved predictive capability, particularly when evaluated at excitation amplitudes different from those used during calibration.

**Table 3** Calibrated parameters of the proposed nonlinear Bouc-Wen Stockbridge damper model tuned on experimental data from Sauter [6].

| | Top mass translation ($i = 1, j = 1$) | Top mass rotation ($i = 1, j = 2$) | Bottom mass translation ($i = 2, j = 1$) | Bottom mass rotation ($i = 2, j = 2$) |
|---|---|---|---|---|
| $k_{ji}^{min}$ | 3700 | 50 | 3700 | 50 |
| $k_{ji}^{max}$ | 12000 | 165 | 12700 | 480 |
| $c_{ji}$ | 0.0011 | 0.0075 | 0.0011 | 0.0075 |
| $a_i$ | 0.001 | – | –0.001 | – |
| $b_i$ | – | –10.5 | – | 10.5 |

## 4 Conclusions

This paper has presented a nonlinear modelling framework for asymmetric Stockbridge dampers intended for vibration mitigation of suspension bridge hangers. The formulation captures the force transmitted at the clamp, as well as an accurate description of the internal damper dynamics, including both translational and rotational motion of the inertial masses. A detailed analysis of the prediction capabilities of the presented model, both in the time and frequency domains, is presented by the authors in [20].

Unlike conventional approaches based on impedance functions identified at a fixed excitation level, the proposed model explicitly accounts for the amplitude-dependent behaviour arising from hysteretic bending of the messenger cables. This enables consistent prediction of response under arbitrary input histories and allows direct coupling with hanger dynamics in time-domain simulations. Model parameters were identified using laboratory measurements performed on a full-scale damper tested in a vertical configuration representative of field installations. The calibrated model reproduces the experimentally observed shifts in resonance frequency and variations in response magnitude across a range of excitation amplitudes. The resulting numerically calculated impedance functions show close agreement with measurements.

Overall, this work offers an experimentally verified nonlinear model capable of capturing both the external force and the internal dynamics of an asymmetric Stockbridge damper for bridge application. Offering a robust basis for the analysis and the design of these devices in a field that differs from the one where they are traditionally employed.

## Acknowledgements

This research was financially supported by the Norwegian Public Roads Administration. The authors appreciate this support.

## References

[1] A. Larsen, “Vibration Excitation and Damping of Suspension Bridge Hanger Cables,” in *Dynamics and Aerodynamics of Cables. ISDAC 2023. Lecture Notes in Civil Engineering*, V. Gattulli, M. Lepidi, and L. Martinelli, Eds. Springer, Cham, 2024, pp. 217–227. doi: 10.1007/978-3-031-47152-0_19.

[2] G. Bacci, Ø.W. Petersen, V. Denoël, and O. Øiseth, “Advanced statistical analysis of vortex-induced vibrations in suspension bridge hangers with and without Stockbridge dampers,” *J. Wind Eng. Ind. Aerodyn.*, vol. 255, no. October, p. 105931, Dec. 2024, doi: 10.1016/j.jweia.2024.105931.

[3] H. Wagner, V. Ramamurti, R. V. R. Sastry, and K. Hartmann, “Dynamics of stockbridge dampers,” *J. Sound Vib.*, vol. 30, no. 2, pp. 207–220, 1973, doi: 10.1016/S0022-460X(73)80114-2.

[4] I. Pivovarov and O. G. Vinogradov, “One application of Bouc’s model for non-linear hysteresis,” *J. Sound Vib.*, vol. 118, no. 2, pp. 209–216, Oct. 1987, doi: 10.1016/0022-460X(87)90521-9.

[5] D. Sauter and P. Hagedorn, “On the hysteresis of wire cables in Stockbridge dampers,” *Int. J. Non. Linear. Mech.*, vol. 37, no. 8, pp. 1453–1459, 2002, doi: 10.1016/S0020-7462(02)00028-8.

[6] D. Sauter, “Modeling the Dynamic Characteristics of Slack Wire Cables in Stockbridge Dampers,” Technischen Universität

Darmstadt, 2003.
[7] F. Foti and L. Martinelli, “Hysteretic Behaviour of Stockbridge Dampers: Modelling and Parameter Identification,” *Math. Probl. Eng.*, vol. 2018, 2018, doi: 10.1155/2018/8925121.
[8] S. Langlois and F. Legeron, “Prediction of aeolian vibration on transmission-line conductors using a nonlinear time history model - Part I: Damper model,” *IEEE Trans. Power Deliv.*, vol. 29, no. 3, pp. 1168–1175, 2014, doi: 10.1109/TPWRD.2013.2291361.
[9] N. Barbieri and R. Barbieri, “Dynamic analysis of stockbridge damper,” *Adv. Acoust. Vib.*, vol. 2012, 2012, doi: 10.1155/2012/659398.
[10] N. Barbieri, R. Barbieri, R. A. da Silva, M. J. Mannala, and L. de S. V. Barbieri, “Nonlinear dynamic analysis of wire-rope isolator and Stockbridge damper,” *Nonlinear Dyn.*, vol. 86, no. 1, pp. 501–512, 2016, doi: 10.1007/s11071-016-2903-1.
[11] N. Barbieri, M. E. Marchi, M. J. Mannala, R. Barbieri, L. de S. V. Barbieri, and G. de S. V. Barbieri, “Nonlinear dynamic analysis of a Stockbridge damper,” *Can. J. Civ. Eng.*, vol. 46, no. 9, pp. 828–835, Sep. 2019, doi: 10.1139/cjce-2018-0502.
[12] X. Luo, L. Wang, and Y. Zhang, “Nonlinear numerical model with contact for Stockbridge vibration damper and experimental validation,” *JVC/Journal Vib. Control*, vol. 22, no. 5, pp. 1217–1227, 2016, doi: 10.1177/1077546314535647.
[13] F. Bogani, A. Sosio, F. Foti, and L. Martinelli, “A reduced hysteretic model of stockbridge dampers,” *Theor. Appl. Mech. - AIMETA 2022*, vol. 26, pp. 417–422, 2023, doi: 10.21741/9781644902431-68.
[14] F. Ikhouane, V. Mañosa, and J. Rodellar, “Dynamic properties of the hysteretic Bouc-Wen model,” *Syst. Control Lett.*, vol. 56, no. 3, pp. 197–205, 2007, doi: 10.1016/j.sysconle.2006.09.001.
[15] Norsk Elektroteknisk Komite, “EN IEC 61897:2020 - Overhead lines Requirements and tests for Aeolian vibration dampers,” 2020.
[16] G. Diana, A. Cigada, M. Belloli, and M. Vanali, “Stockbridge-type damper effectiveness evaluation: Part I - Comparison between tests on span and on the shaker,” *IEEE Trans. Power Deliv.*, vol. 18, no. 4, pp. 1462–1469, 2003, doi: 10.1109/TPWRD.2003.817797.
[17] J. Chan *et al.*, *EPRI Transmission Line Reference Book: Wind-Induced Conductor Motion*. 2009.
[18] IEEE Standards Committee, “IEEE Guide for Laboratory Measurement of the Power Dissipation Characteristics of Aeolian Vibration Dampers for Single Conductors,” 1993.
[19] G. Diana, A. Manenti, C. Pirotta, and A. Zuin, “Stockbridge-type damper effectiveness evaluation: Part II - The influence of the impedance matrix terms on the energy dissipated,” *IEEE Trans. Power Deliv.*, vol. 18, no. 4, pp. 1470–1477, 2003, doi: 10.1109/TPWRD.2003.817798.
[20] G. Bacci, Ø. W. Petersen, V. Denoël, and O. Øiseth, “Bouc-Wen modelling of asymmetric Stockbridge damper for the wind-induced vibration control of suspension bridge hangers,” *J. Sound Vib.*, vol. 626, p. 119617, Mar. 2026, doi: 10.1016/j.jsv.2025.119617.